PLOS | ONE

RESEARCH ARTICLE

A Novel Matrix Protein Hic31 from the Prismatic Layer of *Hyriopsis Cumingii* Displays a Collagen-Like Structure

Xiaojun Liu[1,2,3☯], Shimei Zeng[1☯], Shaojian Dong[1], Can Jin[1], Jiale Li[1,2,3,4]*

1 Key Laboratory of Freshwater Aquatic Genetic Resources, Shanghai Ocean University, Ministry of Agriculture, Shanghai, China, **2** Shanghai Engineering Research Center of Aquaculture (ZF1206), Shanghai Ocean University, Shanghai, China, **3** Shanghai University Knowledge Service Platform, Shanghai Ocean University Aquatic Animal Breeding Center (ZF1206), Shanghai Ocean University, Shanghai, China, **4** E-Institute of Shanghai Universities, Shanghai Ocean University, Shanghai, China

☯ These authors contributed equally to this work.
* jlli@shou.edu.cn

Citation: Liu X, Zeng S, Dong S, Jin C, Li J (2015) A Novel Matrix Protein Hic31 from the Prismatic Layer of *Hyriopsis Cumingii* Displays a Collagen-Like Structure. PLoS ONE 10(8): e0135123. doi:10.1371/journal.pone.0135123

Editor: Gen Hua Yue, Temasek Life Sciences Laboratory, SINGAPORE

Received: June 11, 2015

Accepted: July 18, 2015

Published: August 11, 2015

Data Availability Statement: All gene related files are available from the Genbank database (Accession No. KR534872).

Funding: This work was supported by a grant from the national science and technology support program (2012BAD26B04), the ability improvement project for engineering and technology research center of the Shanghai Municipal Science and Technology Commission (13DZ228050031272657), and the National Natural Science Foundation of China (31272657).

Abstract

In this study, we clone and characterize a novel matrix protein, hic31, from the mantle of *Hyriopsis cumingii*. The amino acid composition of hic31 consists of a high proportion of Glycine residues (26.67%). Tissue expression detection by RT-PCR indicates that hic31 is expressed specifically at the mantle edge. *In situ* hybridization results reveals strong signals from the dorsal epithelial cells of the outer fold at the mantle edge, and weak signals from inner epithelial cells of the same fold, indicating that hic31 is a prismatic-layer matrix protein. Although BLASTP results identify no shared homology with other shell-matrix proteins or any other known proteins, the hic31 tertiary structure is similar to that of collagen I, alpha 1 and alpha 2. It has been well proved that collagen forms the basic organic frameworks in way of collagen fibrils and minerals present within or outside of these fibrils. Therefore, hic31 might be a framework-matrix protein involved in the prismatic-layer biomineralization. Besides, the gene expression of hic31 increase in the early stages of pearl sac development, indicating that hic31 may play important roles in biomineralization of the pearl prismatic layer.

Introduction

Many living organisms are capable of converting inorganic ions into solid minerals through a dynamic physiological process called biomineralization [1, 2]. This process allows the formation of many external and internal hard tissues (e.g. shells, pearls, and bones) that display a wide range of functions [3]. Among biomineralization products, the mollusk shell and pearl (especially the nacre of shells or pearls as a non-human organic-mineral biomaterial) becomes the focus of biomaterial and aquatic research due to their highly-ordered microstructure and superior mechanical properties [2, 4]. The nacre is usually comprised of 95% calcium carbonate and accounts for only 0.1%-5% of the organic matrix, of which the organic matrix are densely

Competing Interests: The authors have declared that no competing interests exist.

packed with proteins, polysaccharides, and lipids [5]. These macro-molecules are secreted by the polarized mantle characterized by three folds among bivalves. The outer epithelial cells in the outer folds of different regions are responsible for nacre deposition and secretion of prism precursors. In general, the outer epithelium of the edge in the outer folds is always related to the formation of prismatic layer, while the dorsal region is always involved in nacreous layer formation. Until now, researchers has revealed that various phases, including nucleation, crystallization, crystal orientation, and crystal morphology, can be influenced by proteins extracted from shell through interactions of protein-mineral, protein-protein, and feedback between macromolecules and crystals [6–17]. Many studies of matrix proteins were focused on seawater mollusks, *pinctada fucata* in particular, from which a majority of proteins have been extracted and identified [15–19], while few matrix proteins from freshwater mollusk have been identified, and the mechanism associated with biomineralization remains unknown.

Hyriopsis cumingii, known for yielding high-quality freshwater pearls, owns a dominating position in the freshwater pearl industry. Statistics indicate that the production of freshwater pearls in China constitutes 95% of that seen throughout the world, and that *H.cumingii* contributes 80% of that total [20]. So far, *H.cumingii* matrix proteins have been primarily studied at proteomics and transcriptomics level [21–28]. Whereas, the extraction and identification of individual proteins is limited reported. A 48kDa protein was extracted from the pearl of *H. cumingii*, providing evidence of vaterite formation [29] and the matrix protein perlucin is reported to be involved in *H.cumingii* nacre formation [30]. Additionally, the *H.cumingii* protein silkmapin is involved in nacreous- and prismatic-layer formation [31]. Furthermore, analysis of the gene α-CA (*HcCA*) from the freshwater pearl mussel *H.cumingii* suggests that *HcCA* can affect shell growth [32].

In order to enhance our understanding of the molecular mechanisms underlying biomineralization, a novel gene, hic31, was extracted from *H.cumingii* and characterized.

Materials and Methods

Animals

Healthy *H.Cumingii*, were harvested from a mussel farm in Jinhua, Zhejiang province, China. Several glass aquariums, filled with circulating, aerated freshwater, were utilized to maintain them at 23 ±2.0°C for 1 week prior to experimentation.

Total RNA extraction and complementary DNA (cDNA) synthesis

Various tissues (marginal mantle, velum craspedon, center mantle, gill, hepatopancres, intestine, kidney, adductor muscle, foot) were sampled and frozen immediately in liquid nitrogen. RNA from these tissues was extracted using TRIzol reagent according to manufacturer's protocol (Invitrogen, Carlsbad, CA, USA), followed by the confirmation of RNA quality (concentration, purity, and integrity) by 1.2% agarose gel electrophoresis. The first strand of cDNA was synthesized in terms of the directions of FastQuant RT Kit with gDNase (TianGen Biotech Co., LTD., Germany).

Identification of hic31 cDNA ends and bioinformatics analysis

According to the residues of MSI 31 ("GGGGG"), a degenerate sense primer F1 (5′ -GGYG GYGGYGGYGGYGGY-3′ , Y = A/T/C/G) for 3' rapid amplification of cDNA ends (RACE) was designed. Then combined with the obtained C-terminal cDNA ends from 3' RACE, a gene-specific antisense primer R1 (5′ -AGCTGGGACACAAGATGGC-3′), was synthesized for 5'-RACE. The full length of hic31 cDNA sequence was obtained by amplification performed with

a SMARTER RACE cDNA Amplification kit and Advantage 2 cDNA Polymerase Mix based on the manual's instructions (Clotech, Palo Alto, CA, USA).

Comparisons of sequence similarity were conducted using the BLAST program from GenBank (National Center for Biotechnology Information, Bethesda, MD, USA(http://www.ncbi.nlm.nih.gov/)); The hic31open reading frame and the translated amino acid sequences were predicted and acquired by ORF Finder (http://www.ncbi.nlm.nih.gov/gorf/gorf.html). The signal peptide was forecasted by SignalP 4.1 Server (http://www.cbs.dtu.dk/services/SignalP/). The physical and chemical characteristics of the predicted protein were estimated by EXPASY ProtParam (http://web.expasy.org/cgi-bin/protparam/protparam)[33]; The trans-membrane structure could be detected by TMHMM Server v.2.0 (Center for Biological Sequence Analysis, Denmark, http://www.cbs.dtu.dk/services/TMHMM/) and potential glycosylation and phosphorylation sites were analyzed using CBS prediction servers (Center for Biological Sequence Analysis, http://www.cbs.dtu.dk/). The secondary and high structure prediction was performed by accessing into Phyre^2 (http://www.sbg.bio.ic.ac.uk/phyre/) [34]. Protein structural domains were predicted by using the Simple Modular Architecture Research Tool SMART(http://smart.embl-heidelberg.de/) [35] and PROSITE (http://prosite.expasy.org/prosite.html) [33];Through TargetP 1.1 Server (Center for Biological Sequence Analysis, Denmark, http://www.cbs.dtu.dk/services/TargetP/), the sub-cellular location of hic31 protein was estimated.

Tissue-specific gene expression and its pattern in pearl sec during early stages of pearl formation

In order to examine the specific expression of hic31 in tissues by qRT-PCR, six individuals were sampled and cDNAs of various tissues were used as templates prepared as described at section 2.2. In addition, 45 individuals (five for each time point) were prepared for expression examination during pearl sac formation and its early development. Optimal primer pairs, which could generate single PCR product and display an amplification efficiency near the theoretical 100%, were screened out by plotting standard curves. The *EF1α* gene from *H. cumingii* was amplified and its expression level acted as an internal standard reference since the gene expression level was verified to be constant among all tissues [36]. qRT-PCR catalyzed by SYBR Premix ExTaq II (Tli RNaseH Plus) (Takara Bio. Inc., Japan), was then performed in triplicate for each template on the CFX96 real-time PCR Detection System (Bio-Rad, Hercules, CA, USA) in a 20μL reaction comprised of 10μL SYBR Premix Ex Taq II (Tli RNaseH Plus) (2×), 0.8μL of each primer (10μM), 1.0μL cDNA (150ng/μL), and 7.4μL RNase-free water. The program was set as follows: 95°C for 3 min, 40 cycles of 95°C for 5 s and 60°C for 30s, followed by a dissociation curve analysis of 5s per step from 65 to 95°C. The cycle threshold (Ct) values of each sample were then analyzed according to the$2^{-\Delta\Delta Ct}$ method [37] to determine relative expression levels in different tissues against *EF1α* gene expression level in the corresponding samples.

In situ hybridization of hic31 in mantle

To determine the hic31exact expression location in mantle, *in situ* hybridization was conducted. The RNA sense and antisense probes of hic31 were first synthesized by the use of T7 or SP6 RNA polymerase respectively, then a rectangular portion of fresh mantle tissue (0.8×0.5cm) was sampled and immediately fixed in 4% paraformaldehyde (freshly prepared using 0.1% DEPC water) for 6 h, followed by at least 20h incubation at 4°C in 20%-25% sucrose. Frozen sections could be prepared through the use of freezing microtome (LeicaCM 1950, Wetzlar, Germany), followed by slicing the tissue to 10μm thickness and mounting the sliced pieces on poly-lysine pretreated slides. *In situ* hybridization was carried out according to

the manufacturer protocol (Enhanced Sensitive ISH Detection Kit, Boster, and Switzerland) with slight changes.

Results

cDNA cloning and sequence analysis

The 3' RACE procedure amplified 1260bp, and 5' RACE obtained a 516bp fragment. The full 1432bp cDNA sequence (Fig 1) of hic31 was determined by combining the two fragments. Sequence analysis reveals that the open reading frame starts at ATG (position 42) and stops at TAG (position 998). The open reading frame encodes a protein of 317 amino acids, with a theoretical molecular weight of 30.7kDa. The predicted amino acids sequence contains a signal peptide from residues 1–18 (Fig 1). Without regard to the signaling peptide, the theoretical molecular weight is 28.8kDa and the isoelectric point is 7.00.

Protein structure prediction

Secondary structure prediction indicated that hic31 is primarily composed of α-helices (Fig 2). Although BLASTP results identified no homology with other shell matrix proteins or any other known proteins, the protein tertiary structure is similar to that of collagen, type I, alpha 1 and alpha 2 (Figs 3 and 4).

Tissue expression and *in situ* hybridization

The hic31 expression level was detected in seven tissues (intestine, adductor muscle, foot, gill, blood, mantle edge, and pallial) by qRT-PCR. The results indicate that hic31 is specially expressed in mantle tissue, and that expression occurs primarily at the edge rather than the pallial region (Fig 5). To confirm the hic31 expression in the mantle tissue, *in situ* hybridization on frozen mantle sections using digoxigenin (DIG)-labeled hic31-specific probes were performed. The results revealed strong signals in the epithelial cells at the mantle edge (Fig 6).

Expression pattern of hic31 during pearl sac formation and early development

The expression of hic31 in pearl sac was detected by qRT-PCR on days 3,6,9,12,19,26,33,45, and77 after insert operation of pearl tablet into *H. cumingii*, the time span mentioned above includes the early development of pearl sac and pearl initially biomineralization.

Data analysis revealed that hic31 expression increased during early stages of pearl sac development between days 3–23 (Fig 7). After day 23, the expression of hic31 significantly decreased, and remained at a relatively low level until day 45. At day 77, no hic31 expression was observed.

Discussion

A novel shell matrix protein, hic31, was identified from mantle of the freshwater mussel, *H. Cumingii*. Sequence composition analysis of amino acids (Table 1) revealed that it had a high proportion of glycine residues (26.67%), and glycine residues are frequently clustered as multiple polyglycine blocks ($(Gly)_n(n>2)$) in the N-terminal region (residues 39–43, block 1; residues 45–51, block 2; residues 65–70, block 3; residues 88–90, block 4). Block 1 and 2 were separated by a serine (Ser).blocks 2 and 3, and blocks 3 and 4 were all subdivided by a methionine (Met)-rich region. The longer poly glycine blocks in other region (residues 201–245) are also frequently subdivided by Met or Ser. These structural characteristics result in a similar distribution pattern of Met and polyglycine blocks, leading to multiple repeats of

```
                                                                                GGAAGGAAACTCCGATAGCGAAATAAGGTACGGACTGAAG   41
ATG AGG ACT GTC ATT CTT TTC GCT ATC GGA GTT TTC GTT CCG GCA GTA CTG TGC CAA TTA  101
M   R   T   V   I   L   F   A   I   G   V   F   V   P   A   V   L   C   Q   L    20
GGC ATG GAA GGA GGT GCA ATG GAC CTG ATG ACG CTC AGC CTT CTG GCC GGC CAG GGA GGC  161
G   M   E   G   G   A   M   D   L   M   T   L   S   L   L   A   G   Q   G   G    40
GGT GGC GGA AGC GGT GGT GGT GGT GGT GGT GGA TTA GAT TCC ATG ATT CCC ATG ATG CTT  221
G   G   G | 1 S   G   G   G   G   G   G   G | 2 L   D   S   M   I   P   M   M   L    60
ATG TCT CAA ATG GGC GGT GGT GGT GGC GGT ATG TCA GAG ATG ATG AGG ACA ATG GCC CTT  281
M   S   Q   M   G   G   G   G   G   G | 3 M   S   E   M   M   R   T   M   A   L    80
ATG AAC ATG ATG CGA TCA AAC GGC GGT GGA AGT AAC GCA GGC CCA ACT ACC CCA CCA CAG  341
M   N   M   M   R   S   N   G   G   G | 4 S   N   A   G   P   T   T   P   P   Q   100
TCC TCG GCA TCA TCT TTC ATG GGC GGA AGC GGA TCT GGG GCG GCG GGG GGT GGC CTT GGC  401
S   S   A   S   S   F   M   G   G   S   G   S   G   A   A   G   G   G   L   G   120
GCC TTG TCC AGT CTG GCT AAT TTG GGC GGA TTG ACC CTG GAC CCG AGG ACA CAA CAC CTG  461
A   L   S   S   L   A   N   L   G   G   L   T   L   D   P   R   T   Q   H   L   140
CAG AGA GAA GGG CTG GGA GTT GAC CCC GCA GTC CAA GCC ATC TTG TGT CCC CAG CTG CAG  521
Q   R   E   G   L   G   V   D   P   A   V   Q   A   I   L   C   P   Q   L   Q   160
TGT CCC CTT CAC CTG CCC TGC GAA AGC GAG CAG CTT TAC ACT CGG GAG TCG AAC TTC GTA  581
C   P   L   H   L   P   C   E   S   E   Q   L   Y   T   R   E   S   N   F   V   180
TGC AAA GGG TGC CCT CGC TGC CGG ATA GAA TCC TCT AAC ATC TTA GGC ATG CTG GCC GCA  641
C   K   G   C   P   R   C   R   I   E   S   S   N   I   L   G   M   L   A   A   200
ATG GGA ATG GGT GGC TCT GGC GGT ATT GCA GGA GAC GGT ATG GGC GGT GCT TTA GGC GGT  701
M   G   M   G   G   S   G   G   I   A   G   D   G   M   G   G   A   L   G   G   220
GGT ATG GGT GGT ATG GGC GGT GGT ATG GGC GGT TCG GGC GGT GCT ATG GAC GGT ATG AGC  761
G   M   G   G   M   G   G   G   M   G   G   S   G   G   A   M   D   G   M   S   240
GGT GGT ATG GGA GGT ATG GGG GCT GGT CTT GAC GCA ATG AAC TCA CCA AGC GGT CCA CAT  821
G   G   M   G   G   M   G   A   G   L   D   A   M   N   S   P   S   G   P   H   260
GCC GGT GGC CAA AGA GGG CCC AGA GGT CGA CCC CCT GGT CAG AGA CCC GGA AAT CGC GCT  881
A   G   G   Q   R   G   P   R   G   R   P   P   G   Q   R   P   G   N   R   A   280
GAC GGC CCC TCT CCA CCT CCG CGT AGC CAA TCT CCA GGG GAA AAC ACG CTT TCT AAA GAA  941
D   G   P   S   P   P   P   R   S   Q   S   P   G   E   N   T   L   S   K   E   300
GGT CCG CCT TCA GAA GCA GCT AAA CCA GGC AGG CCA GCA CAA GGA AAG GCA GCG TAG      998
G   P   P   S   E   A   A   K   P   G   R   P   A   Q   G   K   A   A   *       318
ACGATAGGCAGTGTCATTCACTTGATGTAATACATGCGTATCCTAAGACAAAGGACAAAGGAAACATACATGAATGACAGCTGCCAAGTAACAACCACGATTTGGCAA  1105
TCACATAACTCCCACACGGCAGATCCTTCCTACTATGATTTATAGTTTCCCTTGTTTAGATATTTTATGCAAGAGGAACATTGCGTACCTTTAGTCGATGAATTATTGTCTA  1217
GCTTTGGATGAAGGCGATTTTTTTACGGTTTCAATTTTTTCATATTTAAGTGATACTATTTTGTTATTGTCTTTATTTACAAGTAACACCGGGCTGGTTGTTCGTGAGAGG  1328
TATGAGGCATTTATCACCATTATGACGTTATCATGGACATTTTGTGCGCTGTTTGCATGCATTTCAGAATAAAATGTGCTCATTGTGCCCTGAAAAAAAAAAA  1432
```

Fig 1. cDNA and deduced amino acid sequence of hic31. The putative signal peptide is shown underlined. The putative polyadenylation signal (AATATA) is shown underlined boxed. The cDNA sequence of hic31 has been submitted to Genebank (Accession No. KR534872).

doi:10.1371/journal.pone.0135123.g001

$(Gly)_mX(Gly)_n$(m>1,n>1,where X prefers to Met or Ser). Met is hydrophobic and Ser residues have a hydroxyl group, however, there appears to be no regularity in terms of arrangement of differently-sized poly glycine blocks. In addition, the acidic amino acids, aspartic acid (Asp) and glutamic acid (Glu) always appear separately. The Asp is only surrounded by neutral amino acids while Glu is coupled with neutral or alkaline amino acids. Lysine (Lys) and proline (Pro) is primarily distributed in the C-terminal region of which Lys was

Fig 2. Secondary structure prediction of hic31. Based on the protein sequence of hic22, the secondary structure prediction is performed by Phyre[2]. The amino acids are colored based on the physiochemical properties of the side chains. The regions adopting putative α-helix and β-sheet conformations are represented as green spiral and blue arrow, respectively. The degrees of confidence 0.9 are also indicated by a rainbow color gradient.

doi:10.1371/journal.pone.0135123.g002

presumed to initiate formation of a basic region to enhance interaction with anionic molecules during shell formation, such as CO_3^{2-}[38, 39].

Secondary structure prediction indicates that hic31 tertiary structure is similar to that of collagen, type I, alpha 1 and alpha 2 (Fig 2), but BLASTP identified no shared homology with

Detailed template information

#	Template	Alignment Coverage	3D Model	Confidence	% i.d.	Template Information
1	c1ygvA_	Alignment		100.0	15	**PDB header:**structural protein/contractile protein **Chain:** A: **PDB Molecule:**collagen i alpha 1; **PDBTitle:** the structure of collagen type i. single type i collagen2 molecule: rigid refinment
2	c1y0fB_	Alignment		100.0	16	**PDB header:**structural protein/contractile protein **Chain:** B: **PDB Molecule:**collagen i alpha 2; **PDBTitle:** the structure of collagen type i. single type i collagen2 molecule
3	c3hqvB_	Alignment		100.0	15	**PDB header:**structural protein, contractile protein **Chain:** B: **PDB Molecule:**collagen alpha-2(i) chain; **PDBTitle:** low resolution, molecular envelope structure of type i2 collagen in situ determined by fiber diffraction. single3 type i collagen molecule, rigid body refinement
4	c3bogB_	Alignment		99.2	16	**PDB header:**antifreeze protein **Chain:** B: **PDB Molecule:**6.5 kda glycine-rich antifreeze protein; **PDBTitle:** snow flea antifreeze protein quasi-racemate
5	c3bogA_	Alignment		99.2	16	**PDB header:**antifreeze protein **Chain:** A: **PDB Molecule:**6.5 kda glycine-rich antifreeze protein; **PDBTitle:** snow flea antifreeze protein quasi-racemate
6	c2pneA_	Alignment		99.1	19	**PDB header:**antifreeze protein **Chain:** A: **PDB Molecule:**6.5 kda glycine-rich antifreeze protein; **PDBTitle:** crystal structure of the snow flea antifreeze protein
7	c3boiB_	Alignment		99.1	19	**PDB header:**antifreeze protein **Chain:** B: **PDB Molecule:**6.5 kda glycine-rich antifreeze protein; **PDBTitle:** snow flea antifreeze protein racemate
8	c3boiA_	Alignment		99.1	19	**PDB header:**antifreeze protein **Chain:** A: **PDB Molecule:**6.5 kda glycine-rich antifreeze protein; **PDBTitle:** snow flea antifreeze protein racemate
9	c1nayC_	Alignment		97.9	13	**PDB header:**structural protein **Chain:** C: **PDB Molecule:**collagen-like peptide; **PDBTitle:** gpp-foldon:x-ray structure
10	c2klwA_	Alignment		94.2	7	**PDB header:**de novo protein **Chain:** A: **PDB Molecule:**(pkg)10; **PDBTitle:** solution structure of an abc collagen heterotrimer reveals a2 single-register helix stabilized by electrostatic3 interactions
11	c1k6fB_	Alignment		88.4	17	**PDB header:**structural protein **Chain:** B: **PDB Molecule:**collagen triple helix; **PDBTitle:** crystal structure of the collagen triple helix model [(pro-2 pro-gly)10]3

Fig 3. Detailed information about template in the secondary structure prediction.

doi:10.1371/journal.pone.0135123.g003

collagen. It may be considered that hic31 folds into a similar structure of collagen only. In vertebrates, the biomineralization of hard connective tissues, such as bone, dentin, and cementum, involves the deposition of calcium phosphate within a collagenous matrix [40, 41]. The collagen formed the basic organic frameworks (collagen fibrils) in these tissues and minerals existed both within and outside of the collagen fibrils [42, 43]. For hydroxyapatite formation, non-

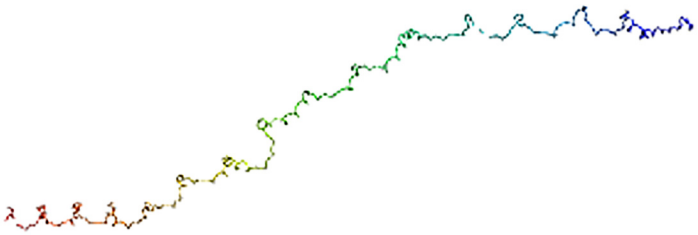

Fig 4. Three dimensional structure prediction of hic31. The tertiary structure prediction is performed by Phyre[2].

doi:10.1371/journal.pone.0135123.g004

collagenous proteins play key roles given that collagen alone does not induce crystal formation [44–46]. This may indicate that hic31 is involved in prismatic layer biomineralization as a framework matrix protein. During the formation of prismatic layer, the organic matrix performs as an organic layer, where newly-formed crystals are embedded. Following this, the inter-prismatic organic membrane of the prismatic layer is produced by squeezing between neighboring crystals [47]. The hic31 may play key roles in this process. Secondary structure prediction also indicated structural similarities between hic31 and antifreeze protein, however, the alignment coverage between the two proteins is narrower than that observed between hic31 and collagen (Fig 3).

Quantitative analysis of *H. cumingii* hic31 expression performed on tissues by qRT-PCR indicated that hic31 is specially expressed in marginal mantle. To determine a more precise expression site of hic31 in the mantle edge, *in situ* hybridization signals were detected on frozen mantle sections. Strong signals were detected in the dorsal epithelial cells of the outer fold at

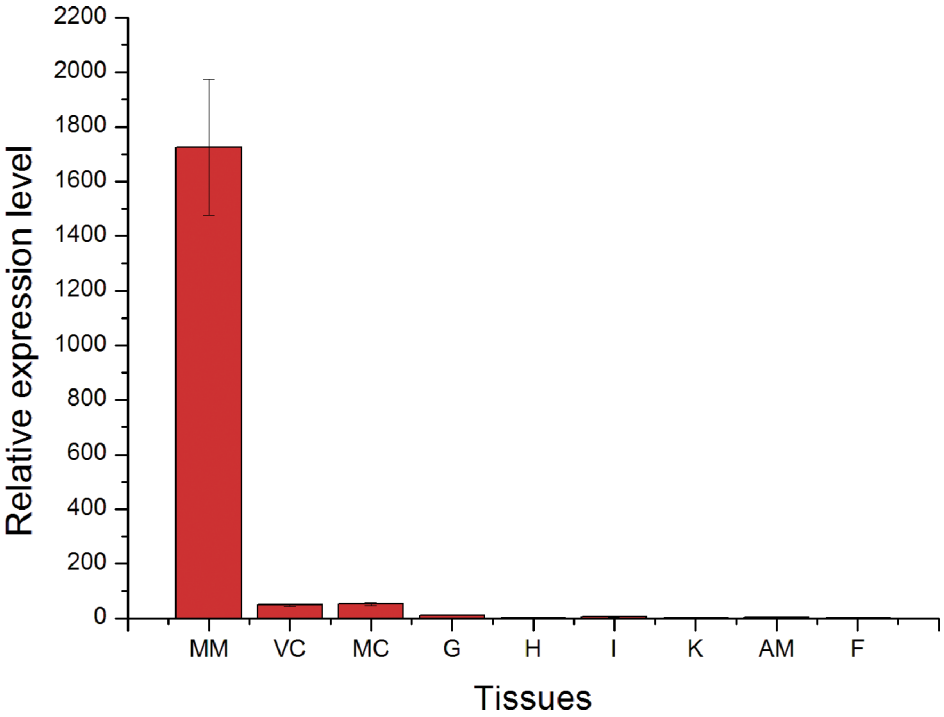

Fig 5. Tissue-specific expression of hic31 by qRT-PCR. MM, Marginal mantle; VC, velum craspedon; CM, Center mantle; G, gill; H, hepatopancres; I, Intestine; K, kidney; AM, adductor muscle; F, Foot.

doi:10.1371/journal.pone.0135123.g005

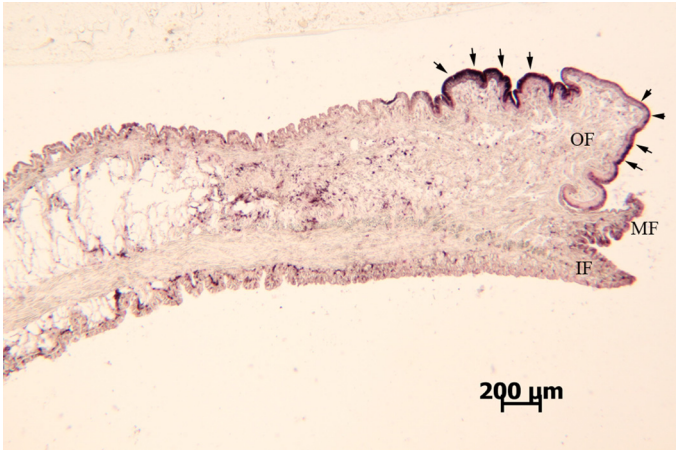

Fig 6. *In situ* hybridization analysis of hic31 gene expression in the mantle of *Hyriopsis cumingii*. IF, inner fold; MF, middle fold; OF, outer fold.

doi:10.1371/journal.pone.0135123.g006

the mantle edge, and weak signals were detected in inner epithelial cells of the outer fold. These results indicate that hic31 is a prismatic layer matrix protein.

The expression of hic31 during early pearl sac development increased significantly during early stages, and decreased obviously following day 23 until no expression was detected on day 77. From previous studies [30, 31, 48], the first nacreous layer has been formed on day 23. The $CaCO_3$, first deposited at the nucleus of calcitic prismatic layer found in the pearl cross-section, followed by nacreous layer formation on the prismatic layer [49, 50]. Therefore, the increased hic31expression from day 3 through day 19 may be responsible for prismatic layer biomineralization, and the period from day 19 to day 23 is a transition time from prismatic layer to nacreous layer biomineralization. Besides, the expression of hic31 decreased significantly after day

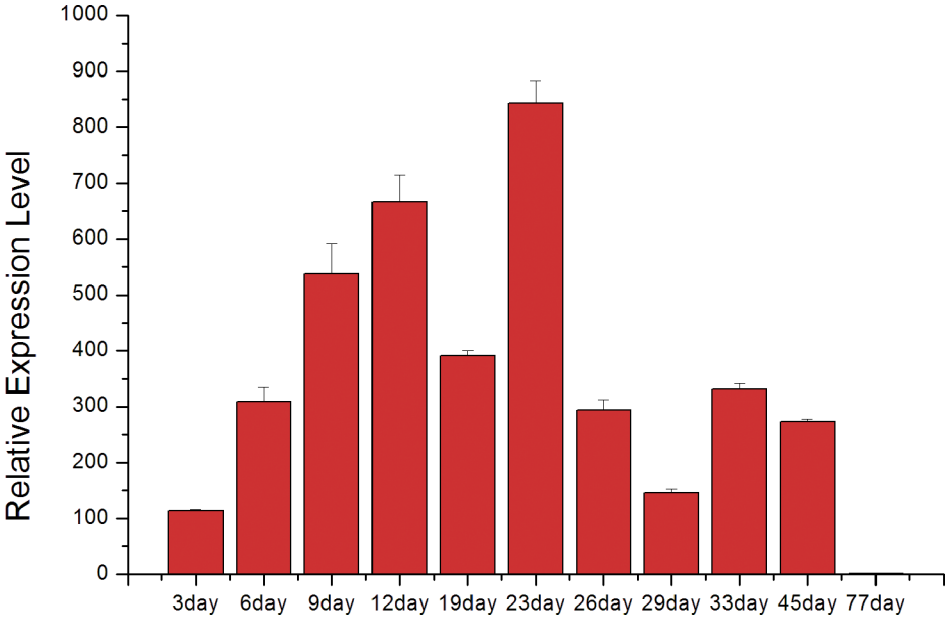

Fig 7. The relative expression level of hic31 in the pearl sac during the early stages of pearl formation after implantation.

doi:10.1371/journal.pone.0135123.g007

Table 1. Amino acid composition (mole percent) of Hic31.

Amino acid	Hic31
Gly (G)	26.67%
Ser (S)	9.67%
Met (M)	9.33%
Leu (L)	8.67%
Ala (A)	8.33%
Pro (P)	8.33%
Arg (R)	4.67%
Gln (Q)	4.67%
Glu (E)	3.33%
Asn (N)	3.00%
Asp (D)	2.67%
Thr (T)	2.67%
Cys (C)	2.00%
Ile (I)	1.67%
Lys (K)	1.33%
His (H)	1.00%
Val (V)	1.00%
Phe (F)	0.67%
Tyr (Y)	0.33%

doi:10.1371/journal.pone.0135123.t001

23, and there was no measureable expression observed when the manner of the nacreous layer biomineralization remains mature and steady. These data suggest that hic31 may play important roles in pearl prismatic layer formation.

Author Contributions

Conceived and designed the experiments: XL JL. Performed the experiments: XL SZ. Analyzed the data: XL SZ JL. Contributed reagents/materials/analysis tools: XL SZ SD CJ. Wrote the paper: XL JL.

References

1. Veis A. The chemistry and biology of mineralized connective tissues. North-Holland, New York: Oxford; 1981.
2. Lowenstam HA, Weiner S. On biomineralization. New York: Oxford University Press; 1989.
3. Simkiss K, Wilbur KM. Biomineralization: cell biology and mineral deposition. San Diego, London: Academic Press; 1989.
4. Weiner S, Gotliv B, Levi-Kalisman Y, Raz S. Biomineralization (BIOM2001): Formation, diversity, evolution and application. Kanagawa: Tokai University Press; 2003.
5. Addadi L, Joester D, Nudelman F, Weiner S. Mollusk shell formation: a source of new concepts for understanding biomineralization processes. Chemistry- A European Journal. 2006; 12: 980–987.
6. Watabe N, Wilbur KM. Influence of the organic matrix on crystal type in mollusks. Nature, 1960; 188:334.
7. Wilbur KM, Watabe N. Experimental studies on calcification in mollusks and the alga *Cocolithus huxleyi*. Ann NY Acad Sci.1963; 109: 82–112. PMID: 14000642
8. Weiner S, Hood L. Soluble protein of the organic matrix of mollusk shells: a potential template for shell formation. Science. 1975: 190, 987–988. PMID: 1188379
9. Addadi L, Weiner S. Interactions between acidic proteins and crystals: stereo-chemical requirements in biomineralization. Proc Natl Acad Sci USA. 1985; 82: 4110–4114. PMID: 3858868

10. Feng QL, Pu G, Pei Y, Cui FZ, Li HD, Kim TN.Polymorph and morphology of calcium carbonate crystals induced by proteins extracted from mollusk shell. Journal of Crystal Growth.2000; 216: 459–465.
11. Thompson JB, Paloczi GT, Kindt JH, Michenfelder M, Smith BL, Stucky G, et al. Direct observation of the transition from calcite to aragonite growth as induced by abalone shell proteins. Biophysics Journal.2000; 79:3307–3312.
12. Mann S. Biomineralization: Principles and concepts in bioinorganic materials chemistry. Oxford: Oxford University Press; 2001.
13. Wheeler AP, George JW, Evans CA. Control of calcium carbonate nucleation and crystal growth by soluble matrix of oyster shell. Science. 1981; 212: 1397–1398. PMID: 17746262
14. Belcher AM, Wu XH, Christensen RJ, Hansma PK, Stucky GD, Morse DE. Control of crystal phase switching and orientation by soluble mollusc-shell proteins. Nature. 1996; 381:56–58.
15. Jiao Y, Wang H, Du XD, Zhao XX, Wang QH, Huang RL. Dermatopontin, a shell matrix protein gene from pearl oyster *Pinctada martensii*, participates in nacre formation. Biochemical and Biophysical Research Communications. 2012; 425: 679–683. doi: 10.1016/j.bbrc.2012.07.099 PMID: 22842462
16. Yan F, Jiao Y, Deng YW, Du XD, Huang RL, Wang QH. Tissue inhibitor of metal loproteinase gene from pearl oyster *Pinctada martensii* participates in nacre formation. Biochemical and Biophysical Research Communications. 2014; 450: 300–305. doi: 10.1016/j.bbrc.2014.05.118 PMID: 24942875
17. Fang D, Pan C, Lin HJ, Lin Y, Zhang GY, Wang HZ, et al. Novel basic protein, PFN23, functions as a key macromolecule during nacre formation. The Journal of Biological Chemistry. 2012; 287:15776–15785. doi: 10.1074/jbc.M112.341594 PMID: 22416139
18. Xiang L, Su JT, Zheng GL, Liang J, Zhang GY, Wang HZ, et, al. Patterns of expression in the matrix proteins responsible for nucleation and growth of aragonite crystals in flat pearls of *pinctada fucata*. Plos One. 2013 Jun 12. doi: 10.1371/journal.pone.0066564
19. Joubert C, Linard C, Le Moullac G, Soyez C, Saulnier D, Teaniniuraitemoana V, et, al. Temperature and food influence shell growth and mantle gene expression of shell matrix proteins in the pearl oyster *pinctada margaritifera*. Plos One. 2014 Aug 14. doi: 10.1371/journal.pone.0103944
20. Wang G, Yuan Y, Li J. SSR analysis of genetic diversity and phylogenetic relationships among different populations of *Hyriopsis cumingii* from the five lakes of China. Journal of fisheries of China.2007; 31: 152–158.
21. Bedouet L, Marie A, Dubost L, Peduzzi J, Duplat D, Berland S, et al. Proteomics analysis of the nacre soluble and insoluble proteins from the oyster *pinctada margaritifera*. Marine Biotechnology. 2007; 9:638–649. PMID: 17641930
22. Bai ZY, Zheng HF, Lin JY, Wang GL, Li JL. Comparative analysis of the transcriptome in tissues secreting purple and white nacre in the pearl mussel *Hyriopsis cumingii*. Plos One, 2013 Jan 14.e53617.doi: 10.1371/journal.pone.0053617 PMID: 23341956
23. Ma Y, Gao Y, Feng Q. Effects of pH and temperature on CaCO3 crystallization in aqueous solution with water soluble matrix of pearls. Journal of crystal Growth. 2010; 312:3165–3170.
24. Ma Y, Gao Y, Feng Q. Characterization of organic matrix extracted from freshwater pearls. Material science & engineering C. 2011; 31:1338–1134.
25. Ma YF, Qiao L, Feng QL. In-vitro study on calcium carbonate crystal growth mediated by organic matrix extracted from fresh water pearls. Material science & engineering C. 2012; 32:1963–1970.
26. Berland S, Ma YF, Marie A, Andrieu JP, Bedouet L, Feng QL, et al. Proteomic and profile analysis of the proteins laced with aragonite and vaterite in the freshwater mussel *Hyriopsis cumingii* shell biominerals. Protein and Peptide Letters.2013; 20: 1170–1180. PMID: 23409939
27. Ren DN, Albert O, Sun MH, Muller WEG, Feng QL. Primary cell culture of fresh water *Hyriopsis cumingii* mantle/pearl sac tissues and its effect on calcium carbonate mineralization. Crystal Growth & Design.2014; 14: 1149–1157.
28. Xiaojun L, Jiale L. Formation of the prismatic layer in the freshwater bivalve *Hyriopsis cumingii*: the feedback of crystal growth on organic matrix. Acta Zoologica. 2015; 96: 30–36.
29. Natoli A, Wiens M, Schroder HC, Stifanic M, Batel R, Soldati AL, et al. Bio-vaterite formation by glycoproteins from freshwater pearls. Micron. 2010; 41: 359–366. doi: 10.1016/j.micron.2010.01.002 PMID: 20171896
30. Lin JY, Ma KY, Bai ZY, Li JL. Molecular cloning and characterization of perlucin from the freshwater pearl mussel, *Hyriopsis cumingii*. Gene. 2013; 526: 210–216. doi: 10.1016/j.gene.2013.05.029 PMID: 23732290
31. Liu XJ, Dong SJ, Jin C, Bai ZY, Wang GL, Li JL. Silkmapin of *Hyriopsis cumingii*, a novel silk-like shell matrix protein involved in nacre formation. Gene. 2015; 555:217–222. doi: 10.1016/j.gene.2014.11.006 PMID: 25447895

32. Ren G, Wang Y, Qin JG, Tang JY, Zheng XF, Li YM. Characterization of a novel carbonic anhydrase from freshwater pearl mussel *Hyriopsis cumingii* and the expression profile of its transcript in response to environmental conditions. Gene. 2014; 546:56–62. doi: 10.1016/j.gene.2014.05.039 PMID: 24853200

33. Gasteiger E, Hoogland C, Gattiker A, Duvaud S, Wilkins MR, Appel RD. et al. Protein Identification and Analysis Tools on the ExPASy Server. The Proteomics Protocols Handbook, Humana Press.2005; 571–607.

34. Kelley LA, Mezulis S, Yates CM, Wass MN, Sternberg MJE. The Phyre2 web portal for protein modeling, prediction and analysis. Nature Protocols. 2015; 10, 845–858. doi: 10.1038/nprot.2015.053 PMID: 25950237

35. Letunic I, Doerks T, Bork P. SMART: recent updates, new developments and status in 2015.Nucleic Acids Res 2014; doi: 10.1093/nar/gku949

36. Bai ZY, Lin JY, Ma KY, Wang GL, Niu DH, Li JL. Identification of housekeeping genes suitable for gene expression analysis in the pearl mussel, *Hyriopsis cumingii*, during biomineralization. Molecular Genetics and Genomics, 2014, 289: 717–725. doi: 10.1007/s00438-014-0837-1 PMID: 24638931

37. Livak KJ, Schmittgen TD. Analysis of relative gene expression data using real-time quantitative PCR and the 2(T) (–Delta Delta C) Method. Methods, 2001; 25:402–408. PMID: 11846609

38. Shen XY, Belcher AM, Hansma PK, Stucky GD, Morse DE. Molecular cloning and characterization of Lustrin A, a matrix protein from shell and pearl nacre of *Haliotis rufescens*, Journal of Biological Chemistry. 1997; 272: 32412–32481.

39. Sarashina I, Endo K. Primary structure of a soluble matrix protein of scallop shell: Implication for calcium carbonate biomineralization. American Mineralogist. 1998; 83:1510–1515.

40. Iijima M, Moriwaki Y, Kuboki Y. Oriented growth of octacalcium phosphate on and inside the collagenous matrix in vitro. Connective tissue research.1995; 33:197–202. PMID: 7554955

41. Beniash E, Traub W, Veis A, Weiner S. A transmission electron microscope study using vitrified ice sections of predentin: Structural changes in the dentin collagenous matrix prior to mineralization. Journal of Structural Biology.2000; 132:212–225. PMID: 11243890

42. Landis WJ, Song MJ, Leith A, Mcewen L, Mcewen BF. Mineral and organic matrix interaction in normally calcifying tendon visualized in 3dimensions by high-voltage electron-microscopic tomography and graphicimage-reconstruction. Journal of Structural Biology. 1993; 110: 39–54. PMID: 8494671

43. Traub W, Arad T, Weiner S. 3-Dimensional ordered distribution of crystals in Turkey tendon collagen-fibers. Proc. Natl. Acad. Sci. USA.1989; 86: 9822–9826. PMID: 2602376

44. Saito T, Arsenault AL, Yamauchi M, Kuboki Y, Crenshaw MA. Mineral induction by immobilized phosphoproteins. Bone, 1997; 21: 305–311. PMID: 9315333

45. Bradt JH, Mertig M, Teresiak A, Pompe W. Biomimetic mineralization of collagen by combined fibril assembly and calcium phosphate formation. Chemistry of Materials.1999; 11: 2694–2701.

46. Hunter GK, Poitras MS, Underhill TM, Grynpas MD, Goldberg HA. Induction of collagen mineralization by a bone sialoprotein-decorin chimeric protein. Journal of Biomedical Material Research. 2001; 55:496–502.

47. Liu XJ, Li JL. Formation of the prismatic layer in the freshwater bivalve *Hyriopsis cumingii*: The feedback of crystal growth on organic matrix. Acta zoologica, 2015; 96: 30–36.

48. Liu X, Li J, Xiang L, Sun J, Zheng G, Zhang G, et al. The role of matrix proteins in the control of nacreous layer deposition during pearl formation. Proc. R. Soc. B Biol. Sci. 2012; 279: 1000–1007.

49. Cuif JP, Ball AP, Dauphin Y, Farre B, Nouet J, Perez-Huerta A, et al. Structural, mineralogical, and biochemical diversity in the lower part of the pearl layer of cultivated seawater pearls from Polynesia. Microscopy and Microanalysis. 2008; 14: 405–417. doi: 10.1017/S1431927608080859 PMID: 18793485

50. Ma HY, Su AA, Zhang BL, Li RK, Zhou LC, Wang BL. Vaterite or aragonite observed in the prismatic layer of freshwater-cultured pearls from South China. Progress in Natural Science. 2009; 19:817–820.